Supporting Information

Crystal-Facet-Dependent Denitrosylation: Modulation of NO Release from *S*-nitrosothiols by Cu_2O Polymorphs

Sourav Ghosh, Punarbasu Roy, Sanjay Prasad and Govindasamy Mugesh*

Department of Inorganic and Physical Chemistry, Indian Institute of Science, Bangalore 560012, India

Table of Contents

Chemicals

All reagents used herein were of analytical grade and used directly without any further purification. Copper (II) chloride dihydrate ($CuCl_2.2H_2O$) and oleic acid were purchased from S. D. Fine Chemicals Pvt. Ltd. Copper sulphate pentahydrate ($CuSO_4.5H_2O$), polyvinylpyrrolidone (PVP K-30), (2-hydroxypropyl)-β-cyclodextrin (β-HCD) were purchased from Sisco Research Laboratories Pvt. Ltd. *D*-Glucose, sodium nitrite ($NaNO_2$), Copper chloride (CuCl), potassium bromide (KBr) glutathione (GSH), *L*-cysteine, *L*-homocysteine, *L*-*N*-acetylcysteine (NAC), *S*-nitroso-*N*-acetyl-*DL*-penicillamine (SNAP), ferrocene, meso-tetraphenylporphyrin cobalt (II) ([(TPP)Co^{II}]) and diethylammonium diethyldithiocarbamate (dtc) were purchased from Sigma-Aldrich. 2,3-Diaminonaphthalene (DAN) was purchased from Alfa Aesar. Ultrapure water was used for all the synthesis and experiments.

Characterization Methods

UV-Vis absorption spectra were acquired on SHIMADAZU UV-2600 spectrophotometer. Fluorescence spectroscopy was measured by using HORIBA JOBIN YVON (Fluoromax – 4 Spectrofluorometer) instrument. X-Ray photoelectron spectroscopy (XPS) analysis was performed by AXIS Ultra, KRATOS ANALYTICAL, SHIMADAZU. Raman spectroscopy measurement was done using Renishaw in-Via Raman Microscope (Renishaw Inc, UK), with excitation wavelength 514 nm. Powder XRD was recorded on Phillips PANalytical diffractometer (using Cu K_α (λ = 1.5406 Å) radiation). Scanning electron microscopy (SEM) and EDX spectra were performed by using FEI Sirion UHR SEM and ESEM-Quanta instruments respectively. Transmission electron microscopy (TEM) and X-ray mapping images recorded on JEOL transmission electron microscope operating at 200 kV after casting a drop of nanoparticle dispersion in isopropyl alcohol over Cu grid. HRTEM and SAED were recorded by using Titan Themis 300kV from FEI. FT-IR spectra were acquired by PerkinElmer FT-IR spectrometer. Brunauer-Emmett-Teller (BET) surface area measurement was performed on Micromeritics surface area analyzer model ASAP 2020. Pore size distribution was calculated by the Barret–Joyner–Halenda (BJH) method. Zeta potential of the materials were recorded on a MALVERN Zetasizer Nano ZS. Electron paramagnetic resonance (EPR) spectroscopy measurement were done a X-band JEOL (JES FA200) instrument. isothermal titration calorimetry (ITC) experiments were performed by using VPITC.

S-nitrosothiol	Molar Extinction Coefficient (mM^{-1} cm^{-1})
SNAP	1.00
GSNO	0.85
SNAC	0.87
HCYSNO	0.73
CYSNO	0.74

Table S1 Molar extinction coefficients (ε) of S-nitrosothiols at 335 nm.[1]

Assay conditions for de-nitrosylation of *S*-nitrosothiols (RSNO)

Substrate	Substrate Concentration (mM)	Cu_2O Concentration (ng μl^{-1})	Buffer	Temperature (ºC)
SNAC	0.75	10	0.1 M sodium phosphate buffer pH 7.4	25
GSNO	0.75	10		
HCYSNO	1.00	10		
SNAP	0.50	2		
CYSNO*	1.00	0.2		

Table S2 Assay conditions for different *S*-nitrosothiols (RSNO).

$$\text{Rate of de-nitrosylation} = \frac{\text{Rate of decrease in the absorbance } (s^{-1})}{\text{Molar extinction coefficient } (M^{-1}\,cm^{-1})} \text{x } 10^9 \text{ nM } s^{-1}$$

* De-nitrosylation of *S*-nitrosocysteine (CYSNO) was monitored using lower concentration of nanomaterials, compared to the concentration used in the case of other RSNOs, due to higher reactivity of *S*-nitrosocysteine.

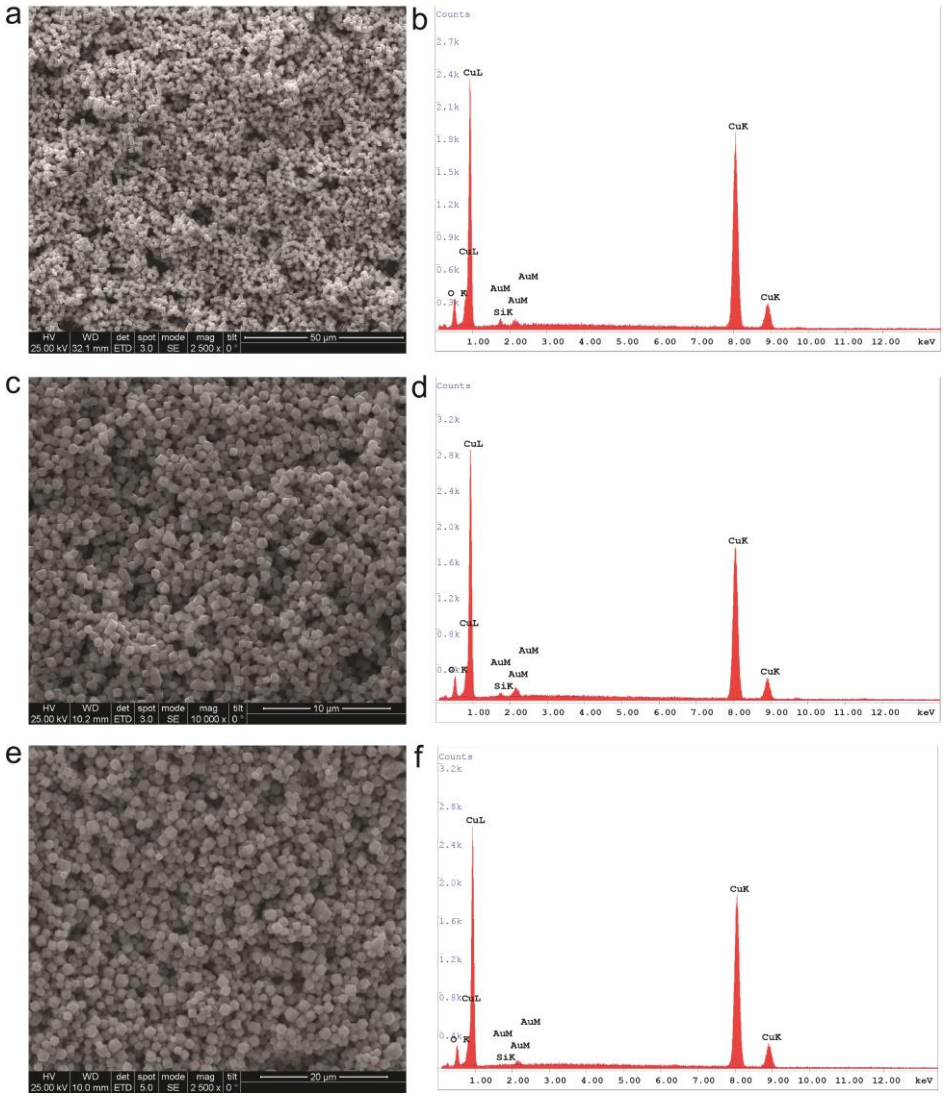

Fig. S1 Energy dispersive spectroscopy (EDS) (right column) of Cu_2O nanomaterials. Low-resolution SEM images (left column) of the area from where EDS spectra was recorded. a, b) cubes, c, d) OH, e, f) RDh. The spectra confirm the elemental purity of the nanomaterials. As samples were drop-casted on silicon wafer and coated with gold before analysis, peaks for gold and silicon are present in the spectra.

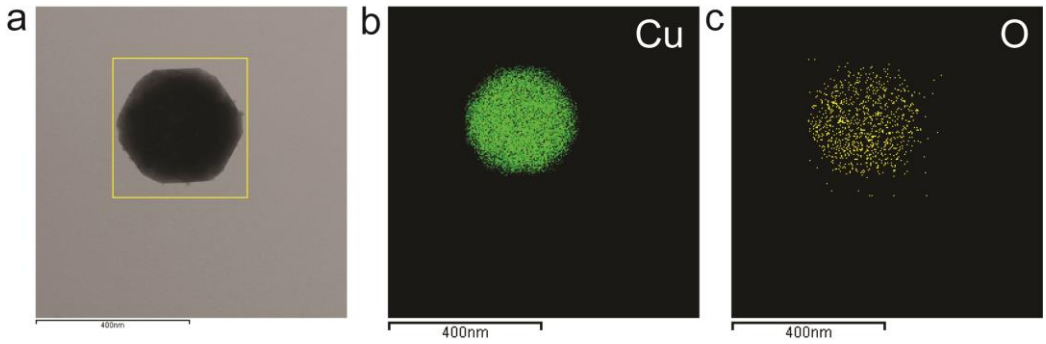

Fig. S2 X-ray mapping images of Cu_2O Oh. a) Selected area bright field (SABF) image and b, c) distribution of copper and oxygen atoms respectively.

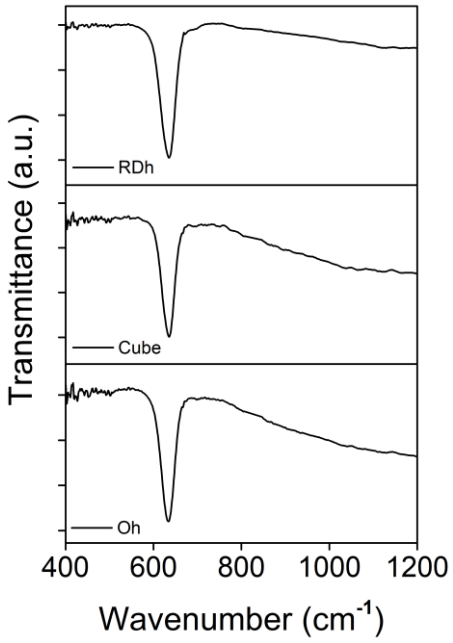

Fig. S3 FT-IR spectra of Cu_2O nanomaterials. The sharp peak at 635 cm^{-1} is due to the stretching vibration of Cu_2-O. Absence of any peak at 540 cm^{-1} confirms that Cu is predominately +1 oxidation states in all the morphologies.

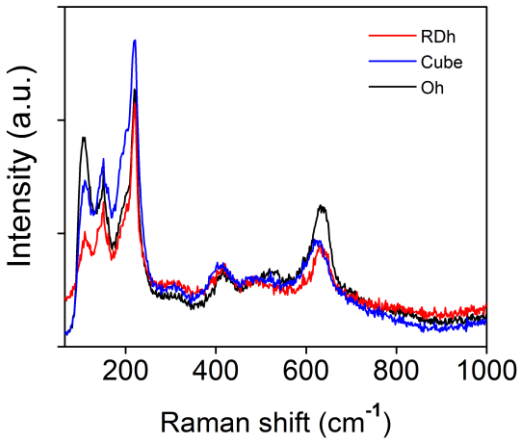

Fig. S4 FT-Raman spectra of Cu_2O nanomaterials.

Vibrational mode	Raman Shift (cm^{-1})		
	RDh	Cube	Oh
$\Gamma^{-}_{(12)}$	109.6	105.0	109.6
$\Gamma_{15}^{-(1)}$ LO	150.8	150.8	150.8
2nd order overtone of $\Gamma^{-}_{(12)}$: $2\Gamma^{-}_{(12)}$	219.5	219.0	219.5
2nd order overtone of $\Gamma_{15}^{-(1)}$: $2\Gamma_{15}^{-(1)}$	309.1	-	-
4th order overtone of $\Gamma^{-}_{(12)}$: $4\Gamma^{-}_{(12)}$	416.0	417.0	416.1
Raman allowed mode Γ_{25}^{+}	521.5	524.0	
$\Gamma_{15}^{-(2)}$ TO	621.0	632.0	630

Table S3 Peaks obtained from Raman spectra of Cu_2O nanomaterials. Experimentally it was observed that the phonon assisted absorption of Cu_2O was predominated by the involvement of $\Gamma^{-}_{(12)}$.[2]

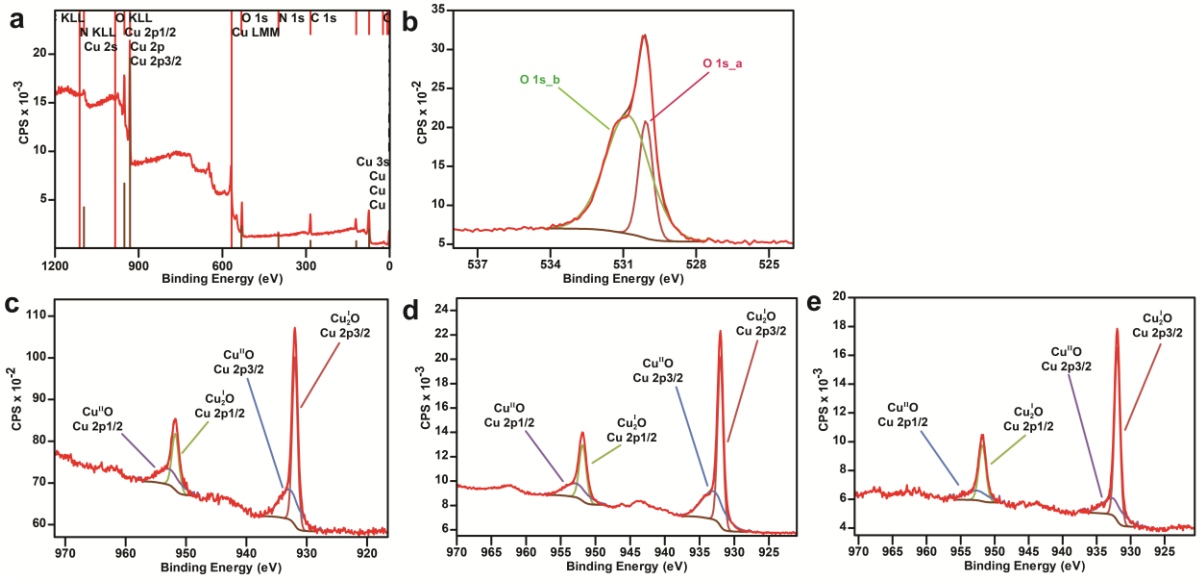

Fig. S5 X-ray photoelectron spectra (XPS) of Cu_2O nanomaterials. The binding energy of C 1s (284.6 eV) was used as standard to calibrate all the spectra. a) Wide spectra of Cu_2O Oh show peaks for Cu and O, which confirms the elemental purity of the sample. Small peaks for C and N are present which might be due to atmospheric carbon and nitrogen. b) Deconvoluted peak of oxygen in Cu_2O Oh. The peak at 530 eV (O 1s_a) is due to Cu-O bond whereas, peak at 530.8 eV (O 1s_b) is due to surface hydroxyl (-OH) groups on the surfaces. c-e) Deconvoluted peak for copper in Cu_2O RDh, Cube and Oh respectively. Though some small peaks are observed at higher binding energy values, no shake-up satellite peaks were observed at 942 eV and 948 eV which rules out the possibility of the formation of mixed oxide. The sharp peaks (with FWHM ~1.00) observed at ~932 eV and the difference in binding energy (ΔBE ~19.8 eV) between Cu 2p3/2 and Cu 2p1/2 for all the nanomaterials confirms that copper atoms are in +1 oxidation states.[3]

		RDh	Cube	Oh
Cu (I) 2p3/2	Binding Energy (eV)	931.96	932.00	931.97
	FWHM	1.05	0.94	0.97
Cu (II) 2p3/2	Binding Energy (eV)	932.77	932.99	932.43
	FWHM	4.10	4.00	3.75
Cu (I) 2p1/2	Binding Energy (eV)	951.76	951.83	951.80
	FWHM	1.37	1.19	1.23
Cu (II) 2p1/2	Binding Energy (eV)	952.71	952.75	952.61
	FWHM	4.52	4.00	3.94
O 1s_a	Binding Energy (eV)			530.06
	FWHM			0.68
O 1s_b	Binding Energy (eV)			530.82
	FWHM			2.15

Table S4 Binding energies and full width half maxima (FWHM) of deconvoluted copper and oxygen peaks in XPS.

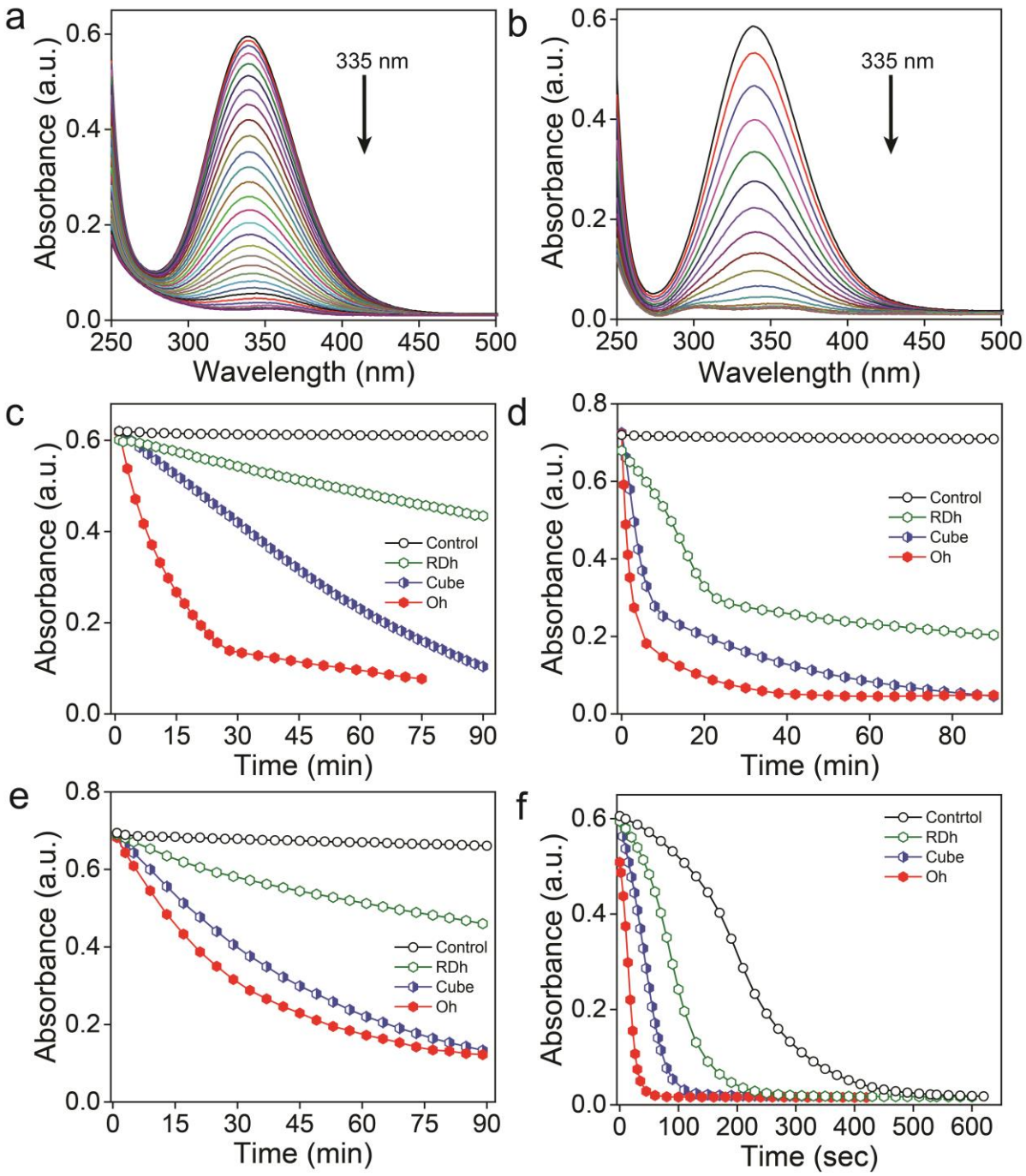

Fig. S6 Monitoring de-nitrosylation of *S*-nitrosothiols using UV-Vis spectroscopy. a, b) UV-Vis spectra recorded during de-nitrosylation of SNAP by Cube and Oh. The absorbance at 335 nm, corresponding to *S*-nitrosothiols decreases over time during de-nitrosylation. c-f) Monitoring Cu_2O nanomaterial mediated de-nitrosylation of GSNO, SNAC, HCYSNO, and CYSNO respectively, over time. Initial rates of the reactions were calculated using the slope in these plots. In the absence of Cu_2O nanomaterials (Control), *S*-nitrosothiols undergo de-nitrosylation very slowly.

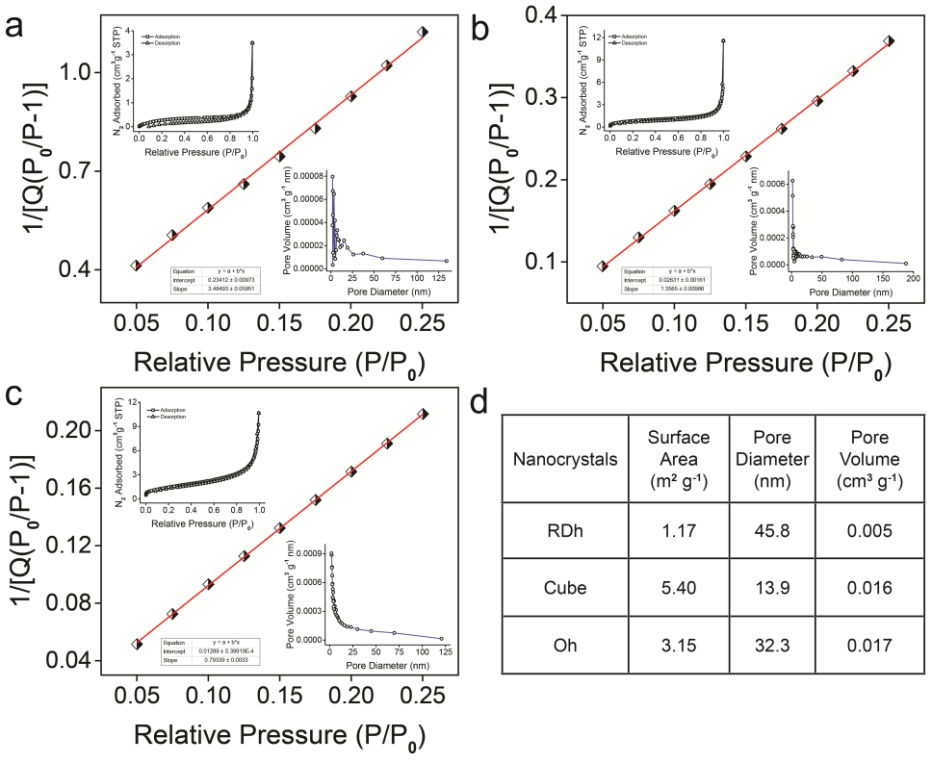

Nanocrystals	Surface Area ($m^2 g^{-1}$)	Pore Diameter (nm)	Pore Volume ($cm^3 g^{-1}$)
RDh	1.17	45.8	0.005
Cube	5.40	13.9	0.016
Oh	3.15	32.3	0.017

Fig. S7 Surface area measurement of Cu_2O nanomaterials by N_2 adsorption and desorption. BET plot, adsorption-desorption isotherm (upper inset) and pore size distribution (lower inset) of a) RDh, b) Cube, c) Oh. d) Surface area, pore diameter and pore volume of three morphologies of Cu_2O nanomaterials.

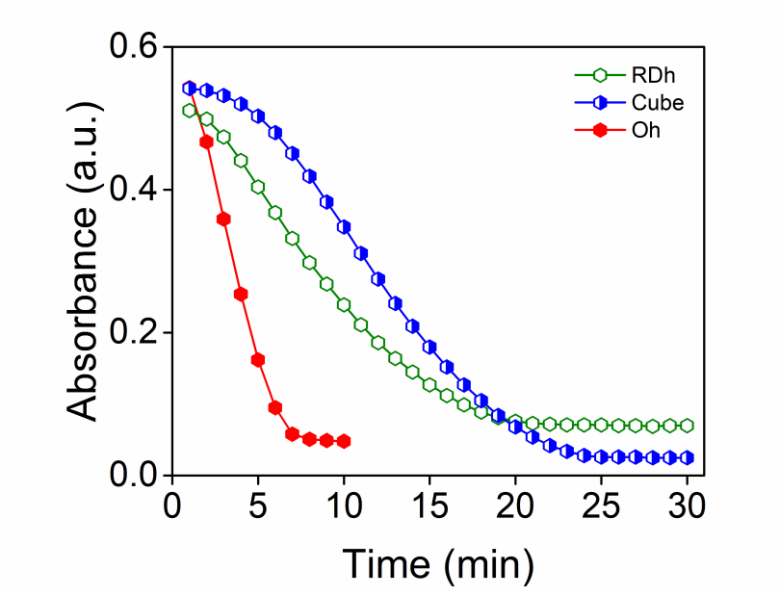

Fig. S8 Comparison of de-nitrosylation activity of different morphologies of Cu_2O nanomaterials after normalizing the concentration of nanomaterials based on surface area obtained from BET measurements i.e. concentration of nanomaterials in the reaction mixture was adjusted such that net surface area is same for three morphologies. Reactions were carried out in 25ºC in 0.1 M phosphate buffer with SNAP (500 µM) as substrate.

Detection of nitric oxide by fluorescence spectroscopy

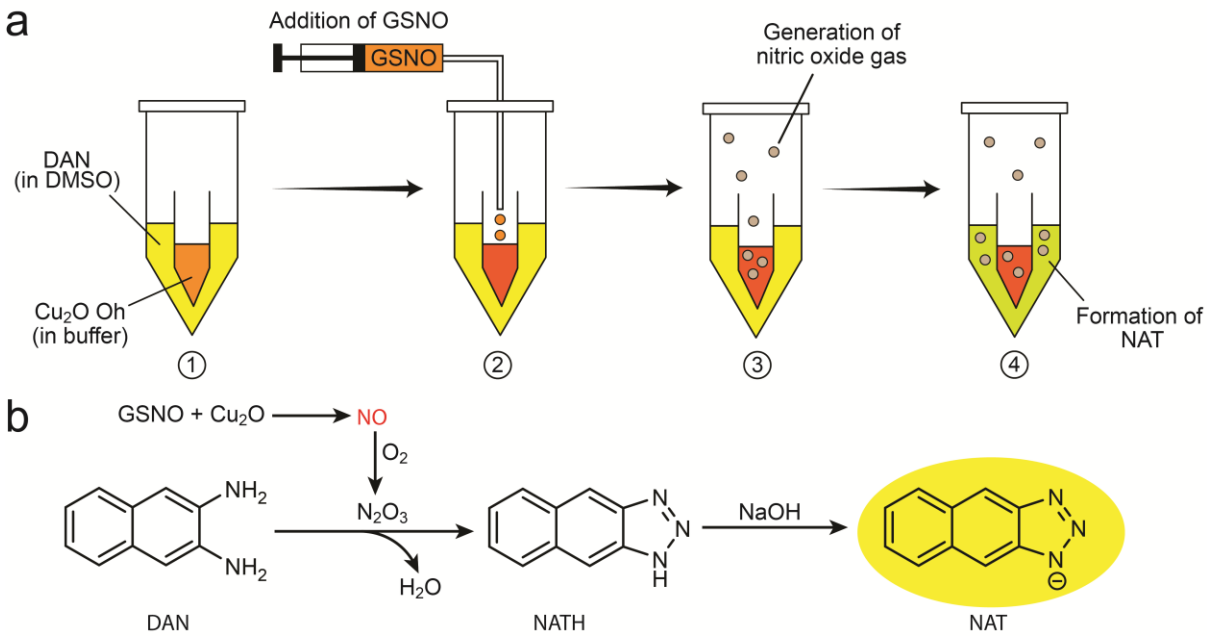

Fig. S9 a) Schematic representation of the experiment setup and the steps involved in the assay. b) reaction scheme for the formation of 2,3-naphthotriazole anion (NAT) from 2,3-Diaminonaphthalene (DAN).

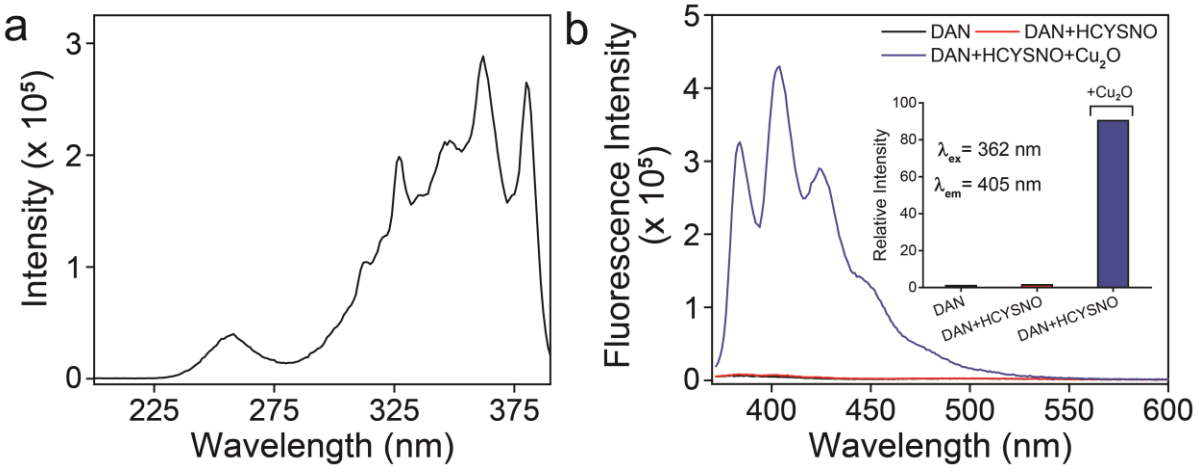

Fig. S10 a) Excitation spectra with the excitation maxima at 362 nm. b) Fluorescence spectra of the alkaline solutions of DMSO+H_2O mixture (**Black**: HCYSNO and Cu_2O both absent in the buffer, **Red**: HCYSNO present but Cu_2O absent in buffer; HCYSNO is stable *S*-nitrosothiols and does not release nitric oxide quickly on its own. **Blue**: HCYSNO and Cu_2O both present in buffer). Strong fluorescence indicated the release of nitric oxide (NO) from HCYSNO which in turn results in the formation of NATH when both HCYSNO and Cu_2O nanomaterials were present in the buffer (Inset: relative fluorescence intensities).

Quantification of nitric oxide during denitrosylation of GSNO

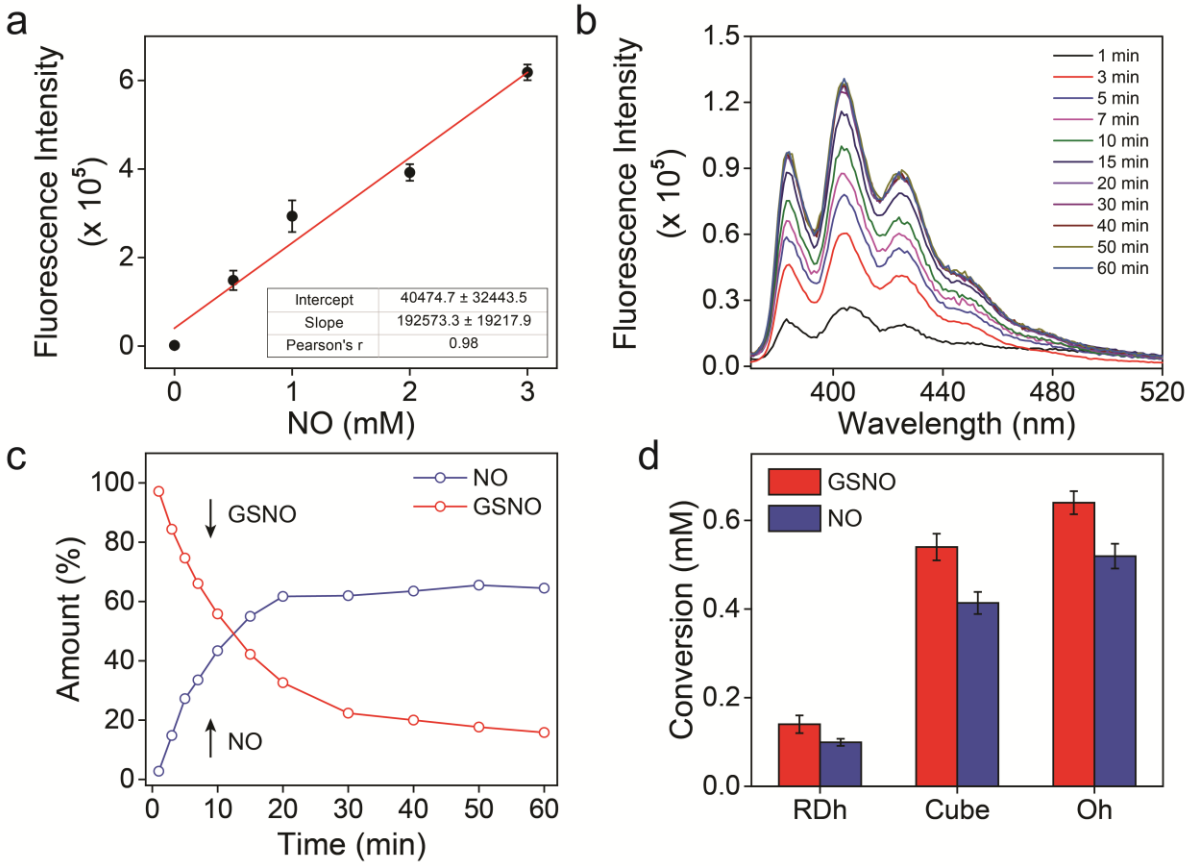

Fig. S11 Quantification of NO using DAN-based fluorescence assay. a) Calibration curve for quantification of NO. Assay conditions: GSNO = 0 - 3 mM, CuCl = 100 µM, DAN = 10 mM, reaction time = 90 min. b) Monitoring the release of NO over time using DAN-based fluorescence assay. Assay condition: GSNO = 0.75 mM, Cu_2O Oh = 10 ng μL^{-1}, DAN = 10 mM. The intensity of the emission (λ_{exc} = 362 nm, λ_{em} = 405 nm) increases with time, indicating the release of NO during denitrosylation. Amount of NO released, which is the same as amount of NATH formed, was calculated using the fluorescence intensity at 405 nm and the calibration plot. c) Simultaneous denitrosylation of GSNO and release of nitric oxide over time. Conversion of GSNO and NO calculated from UV-vis assay and DAN-based fluorescence assay, respectively. d) A comparison of the extent of denitrosylation of GSNO and corresponding amount of NO released by Cu_2O nanocrystals after 75 mins of reaction. Clearly, all the morphologies of Cu_2O nanocrystals convert most of the GSNO to NO during denitrosylation.

Detection of nitric oxide by EPR spectroscopy

$(dtc)_2Fe^{II}$ was used to probe nitric oxide by EPR spectroscopy. A smaller Eppendorf (0.75 ml) containing GSNO (20 mM in 0.1 M phosphate buffer pH 7.4) and Cu_2O nanomaterials (50 ng μl^{-1}) was placed carefully inside a bigger Eppendorf (5 ml) containing $(dtc)_2Fe^{II}$ (in CH_2Cl_2) so that the two solutions remain separated. The bigger Eppendorf was shaken occasionally and incubated for 45 mins. After that the smaller Eppendorf was taken out carefully, 200 µl of solution from the bigger Eppendorf was transferred to a quartz EPR tube and analysed by X-band EPR spectroscopy. The room temperature EPR spectrum exhibits three lines that confirm the formation of $(dtc)_2FeNO$ complex. $(dtc)_2FeNO$ species generated upon reaction with NO-gas released from the reaction mixture of inner Eppendrof and diffuses into the bigger Eppendrof conatining $(dtc)_2Fe^{II}$ complex in dichloromethene.

Conditions used during EPR-spectroscopy measurement: Central field = 336.0 mT, mod. width = 1.0*1 mT, sweep width = 5*10 mT, time constant = 0.03 s.

NO-source	NO-complex	Frequency (MHz)	g-value
GSNO + Cu_2O	$(dtc)_2FeNO$	9448.8	g1=2.018, g2=2.010, g3=2.002
GSNO		9453.4	g1=2.018, g2=2.008, g3=2.002

Table S5 Frequencies and g-values obtained from the EPR spectra.

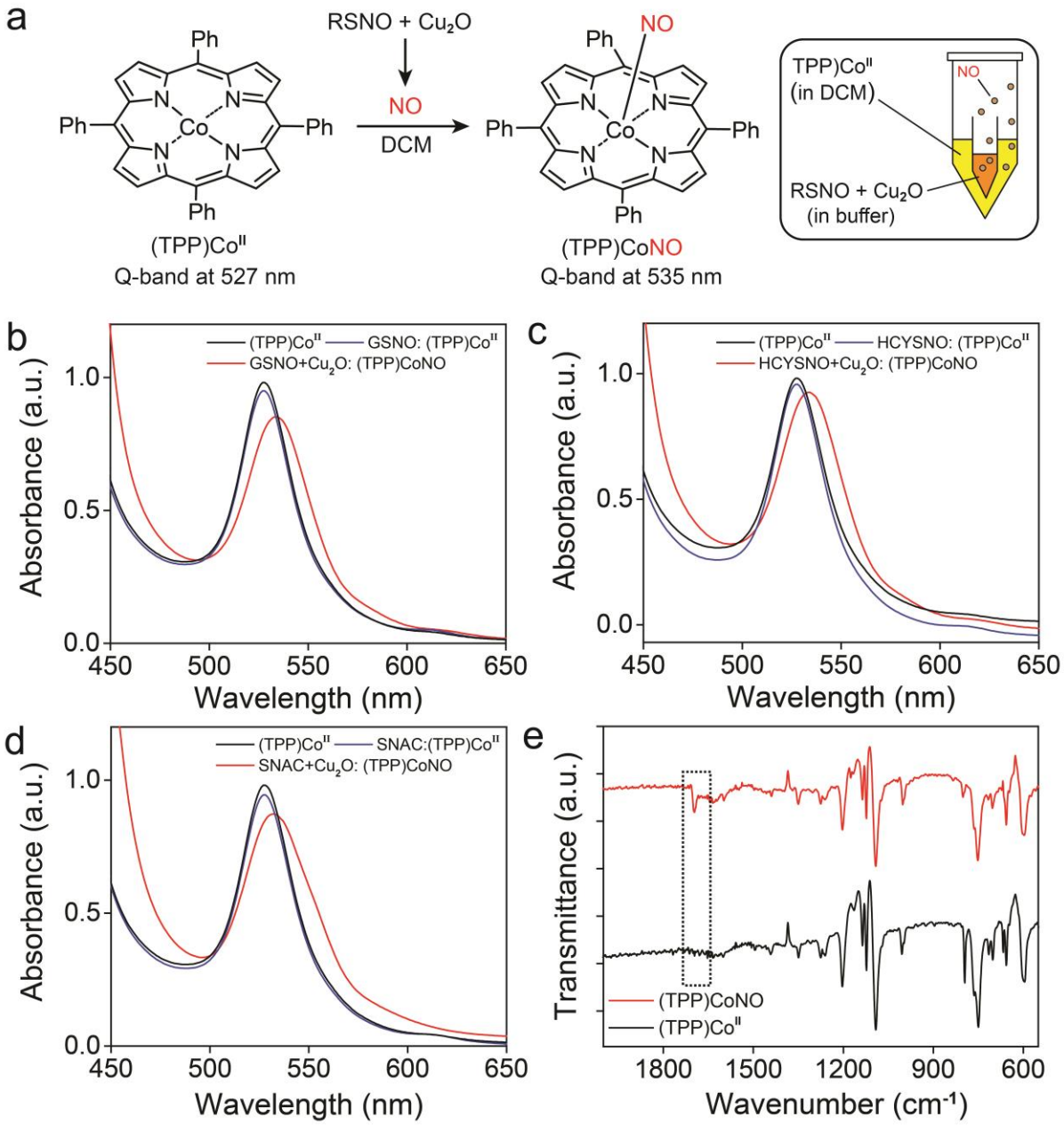

Fig. S12 a) Schematic representation of the trapping of NO by (TPP)Co^{II} complex. b, c and d) UV-Vis spectra of the DCM solutions using GSNO, HYSNO and SNAC as nitric oxide source respectively (**Black**: in the absence of Cu_2O nanomaterials as well as RSNO in buffer, **Blue**: RSNO present but Cu_2O nanomaterials absent in buffer, **Red**: RSNO and Cu_2O nanomaterials both present in buffer). In the absence of either RSNO or Cu_2O nanomaterials, no shift in the Q-band was observed. **Black**: RSNO and Cu_2O both absent in the buffer. In the absence of Cu_2O, all three *S*-nitrosothiols (GSNO, HCYSNO and SNAC) were stable and did not release NO. e) Confirmation of the presence of metal complex bound nitric oxide using FT-IR spectroscopy. The peak at 1696 cm^{-1} corresponds to N=O stretching of (TPP)CoNO. The peak is absent in native metal complex i.e. (TPP)Co^{II}. This again proves the release of NO from *S*-nitrosothiols (RSNO) in presence of Cu_2O nanomaterials.

Naked eye detection of nitric oxide

Similar experimental set-up was designed as described in the previous section for the detection of NO. A smaller Eppendorf (0.75 ml) containing GSNO (20 mM in 0.1 M phosphate buffer pH 7.4) and Cu_2O nanomaterials (50 ng μl^{-1}) were placed carefully inside a bigger Eppendorf (5 ml) containing β-HCD-Fc (in H_2O) so that the two solutions remain separated (Tube **C+G**). The reaction was incubated for 45 mins for the generation of nitric oxide gas which diffuses in to the solution of the outer vial and reacts with β-HCD-Fc to form β-HCD-Fc^+. After 45 mins, a dark blue coloured layer (iii in Figure S12b) could be observed at the top of the outer solution which indicated the formation of β-HCD-Fc^+ which was further confirmed from the UV-vis spectrum of the outer solution where the characteristic peak for β-HCD-Fc^+, at 618 nm, was observed. As controls, two reactions were carried out, one in the absence of GSNO and Cu_2O both (Tube **B**) and another in the absence of only Cu_2O (Tube **G**). In both control experiments, no blue layer was visible on top of the outer solution and in the UV-vis spectra only one major peak was observed at 428 nm corresponding to yellow coloured β-HCD-Fc but no significant peak for β-HCD-Fc^+ at 618 nm.

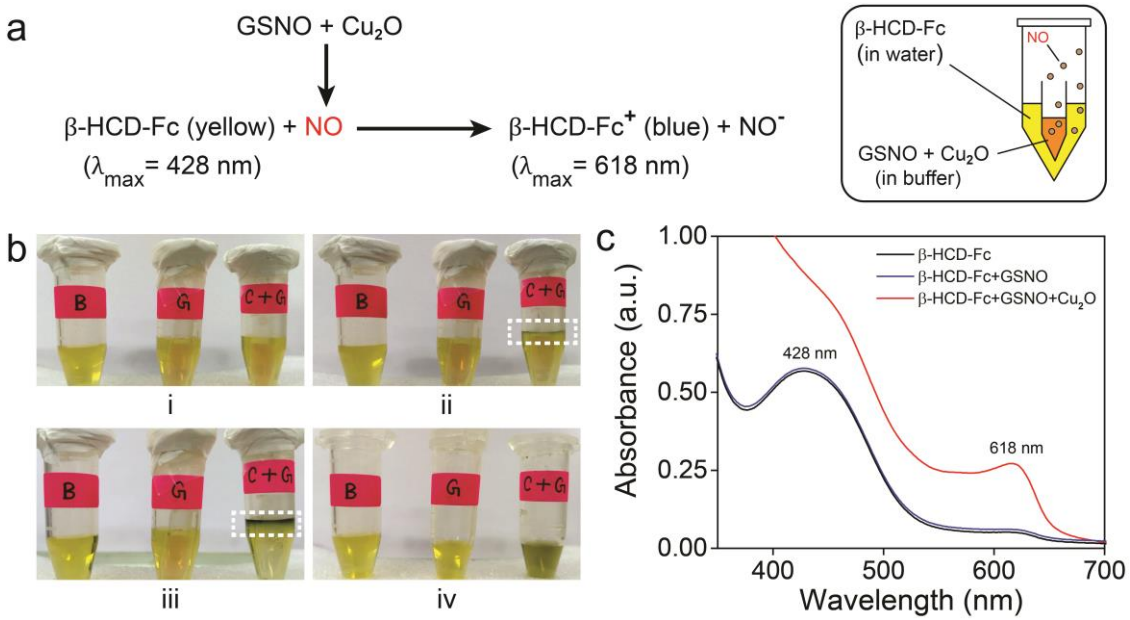

Fig. S13 a) Scheme for the reaction between ferrocene entrapped in cyclodextrin (β-HCD-Fc) and nitric oxide which leads to formation of β-HCD-Fc^+ (blue). b) Formation of a visible layer of β-HCD-Fc^+ (highlighted) in the reaction mixture over time (i: 5 mins, ii: 15 mins, iii: 45 min, iv: after removing the inner Eppendorf vial from the outer one and dispersing the blue coloured band). Only in the case of **C+G**, a visible blue layer was observed, and it turned to became dark over time. This confirms the release of NO and it is detectable by naked eye. and c) UV-Vis spectra of the outer solution from all three vials, recorded after 45 mins of incubation (**Black**: **B**, **Blue**: **G**, **Red**: **C+G**). The spectra of the outer solution from only **C+G**, has characteristic peak of β-HCD-Fc^+ at 618 nm.

Confirmation of glutathione disulphide (GSSG) as by-product by glutathione reductase (GR) assay

After confirming nitric oxide as one of the products from Cu_2O nanomaterials catalysed de-nitrosylation of RSNO, an assay, using GSNO as the model substrate for de-nitrosylation, was devised to find out the probable by-product. 0.5 mM GSNO was incubated with catalyst (Cu_2O Oh: 10 ng μl^{-1}) in 0.1 M phosphate buffer pH 7.4 at 25°C for 45 mins. Once incubation was over, the reaction mixture was centrifuged to remove the catalyst and collected the supernatant solution. After adding GR (0.25U) and NADPH (0.2 mM) in the supernatant, absorbance of the solution at 340 nm (corresponding to NADPH) was observed using UV-vis spectroscopy. Another solution was made by incubating only 0.5 M GSNO in buffer solution without catalyst in buffer for 45 mins which was used as control. In this assay, GR uses oxidised glutathione (GSSG) as a substrate and convert it to its reduced form (GSH) using NADPH as a cofactor. Activity of GR can be monitored by following the decrease of the absorbance of NADPH over time at 340 nm. Another control experiment was performed where GR was not added in the final step. If the catalyst (Cu_2O nanomaterials) mediated nitric oxide release from *S*-nitrosothiols is accompanied by formation of glutathione disulphide (GSSG), then glutathione reductase (GR) will convert the GSSG into GSH taking electron from NADPH which in turn gets converted into $NADP^+$. In our experiment, we do observe a constant decrease in the absorbance at 340 nm over the course of 5 mins which confirms the formation of glutathione disulphide (GSSG) as a by-product in the de-nitrosylation of RSNO by Cu_2O catalysts.

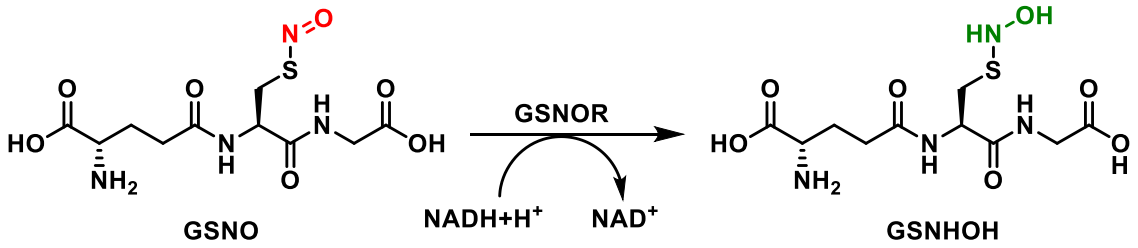

Fig. S14 Conversion of GSNO to GSNHOH by GSNOR using NADH as cofactor. This kind of activity is not shown by the Cu_2O nanomaterials.

In the control reaction, where glutathione reductase was not present, absorbance at 340 nm did not decrease significantly which confirmed Cu_2O nanomaterials can't mimic GSNO Reductase (GSNOR) which converts GSNO to GSNHOH using electrons from NADH/NADPH.

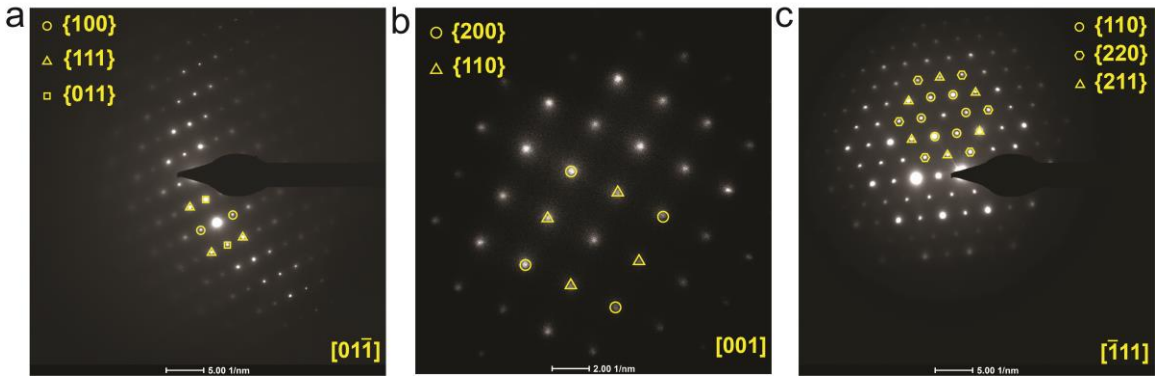

Fig. S15 SAED patterns of Cu_2O nanomaterials. a) RDh, b) Cube, c) Oh.

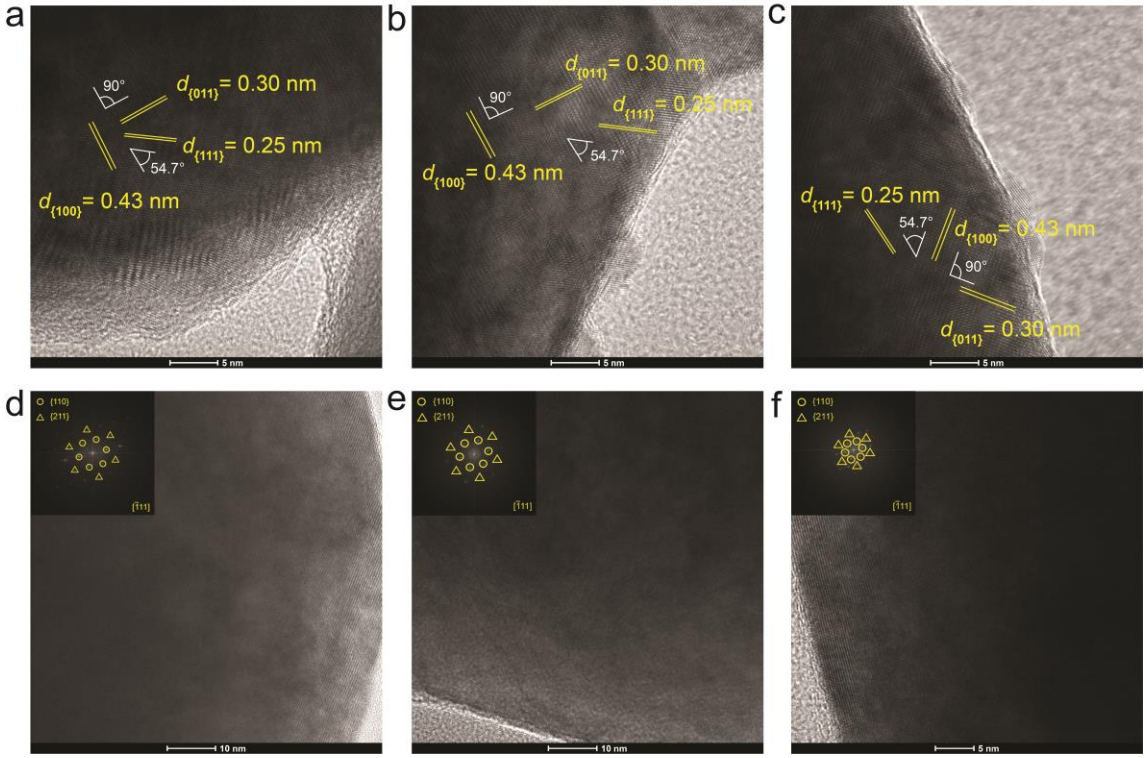

Fig. S16 High resolution TEM (HRTEM) images and Fast-Fourier Transform (FFT) of Cu_2O nanomaterials. a-c) RDh, d-f) Oh.

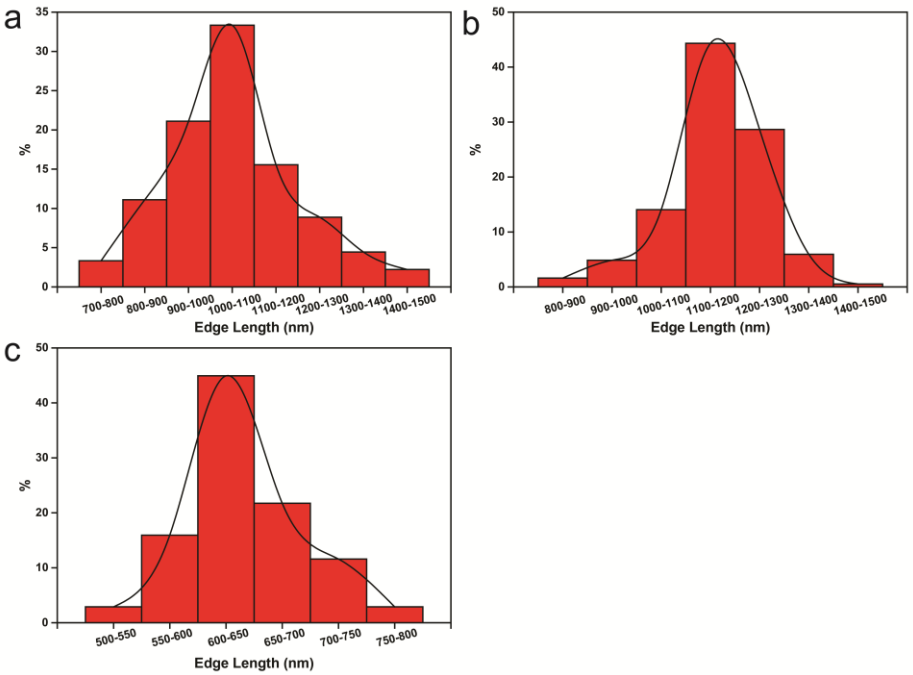

Fig. S17 Size distribution of Cu_2O nanomaterials based on edge length. a) RDh, b) Cube, c) Oh. Average edge length is used to calculate the volume and surface area of single nanoparticles.

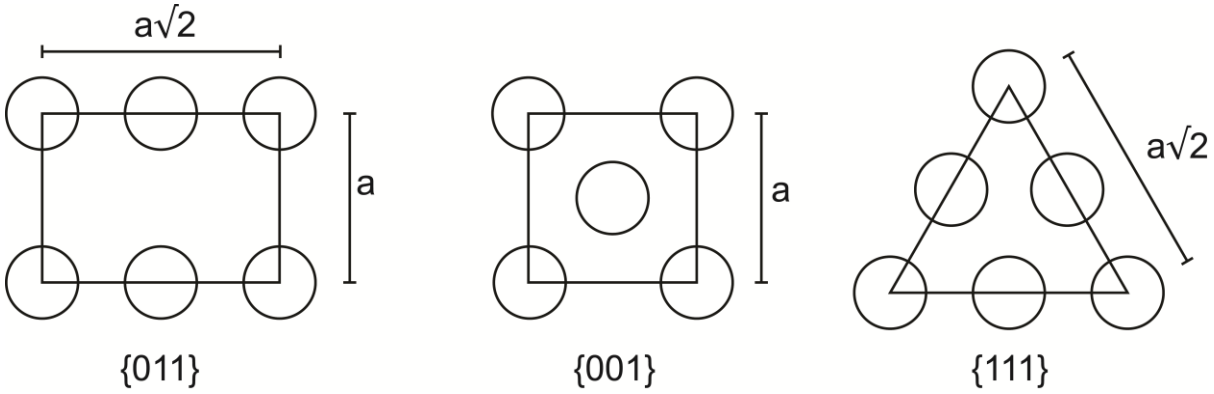

Fig. S18 Arrangement of Cu atoms on different planes of Cu_2O lattice.

	Volume	Planar Density of Cu Atoms
RDh	$\frac{16d^2\sqrt{3}}{9}$	$\frac{2}{a^2\sqrt{2}}$
Cube	d^3	$\frac{2}{a^2}$
Oh	$\frac{d^3\sqrt{2}}{3}$	$\frac{4}{a^2\sqrt{3}}$
a = 4.267 Å (JCPDS 78-2076), d = edge length of nanoparticle		

Table S6 Expressions of surface area, volume and planar density of copper atoms on the surface of nanomaterials, in terms of lattice parameter (a) and edge length (d).

	Edge Length (nm)	Volume (10^{-19} x m^3)	Area (10^{-12} x m^2)	Number of Units (x10^5)	Net Surface Area (10^{-6} x m^2)	Planar Density (x 10^{18} m^{-2})	Number of Copper Atoms on the Surface (x10^{13})	Upscaling Factor
RDh	949.8±144.6	26.3	10.20	1.26	1.29	7.77	1.00	1.89
Cubes	1162.3±101.5	15.70	8.11	2.12	1.72	10.98	1.89	1.00
Oh	642.7±54.1	1.25	1.43	26.6	3.80	12.68	4.83	0.39

Table S7 Estimation of number of Cu atoms on surface of Cu_2O nanomaterials.

Number of nanoparticles in reaction mixture (N) was determined using the following equation,

$$N = \frac{\text{Amount of Copper (I) Oxide}}{\text{Density of Copper (I) Oxide}} \times \frac{1}{\text{Volume of individual units}} \quad \text{(Equation 1)}$$

Density of Copper (I) Oxide was taken as 6 g cm^{-3} i.e. 6000 Kg m^{-3} and for a standard assay, the amount of Copper (I) Oxide in 1 mL was 2 µg i.e. $2*10^{-9}$ Kg. Volume of individual nanoparticle was calculated using the formulas mentioned in Table S6. Net surface area was calculated by multiplying surface area of a single nanoparticle unit by the total number of nanoparticles in solution. Total number of copper atoms on the surface of the nanoparticles was calculated by multiplying the net surface area with planar density of copper atoms and this number was used to calibrate the number or surface copper atoms present in the reaction mixture.

$$\text{Net Surface Area} = \text{N x Surface area of single nanoparticle}$$

$$\text{Number of Copper Atoms on the Surface} = \text{Net Surface Area x Planar Density}$$

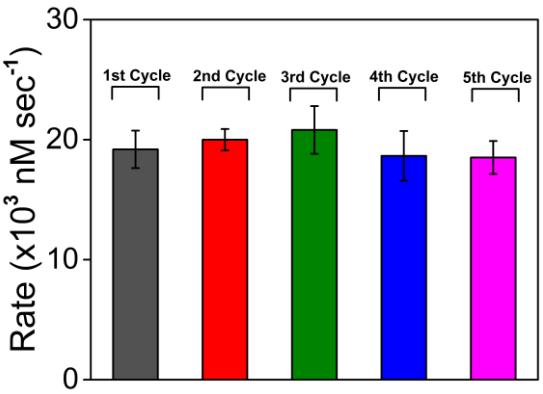

Fig. S19 Recyclability of nanomaterials for the catalysis was checked by measuring the rate of de-nitrosylation after addition of fresh substrate up to 5 times. Assay conditions: 1.0 mM CYSNO, 0.2 ng μL^{-1} Cu_2O octahedra, 0.1 M sodium phosphate buffer pH 7.4, 25°C. Fresh CYSNO was added in the reaction mixture immediately after completion of each cycle. No significant change in the initial rate of de-nitrosylation was observed as the nanomaterials retained their activity throughout multiple cycles indicating the robustness of these materials.

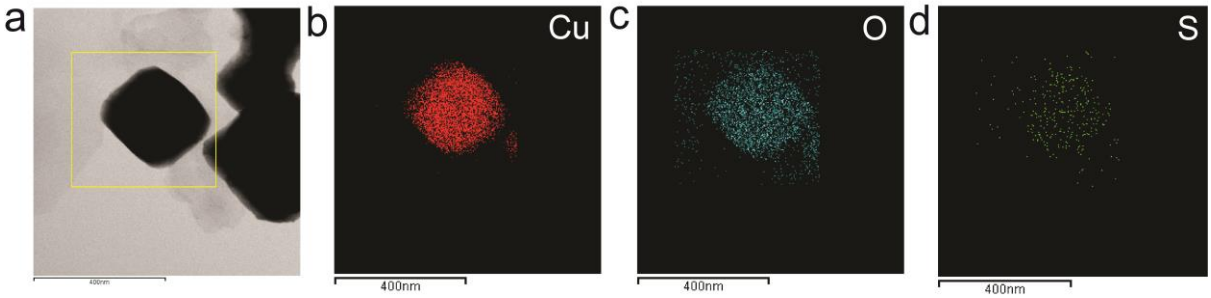

Fig. S20 X-ray mapping images of Cu_2O Oh after the catalysis: a) Selected area bright field (SABF) image of Oh. b), c) and d) Distribution of copper, oxygen and sulphur atoms respectively. Results indicate that the structure and morphology of the Cu_2O Oh is intact even after catalysis and the weak signals of sulphur atoms can be due to the sulphur (from RSNO or RSSR) bound to nanoparticle surface. This indicates that Cu atoms on the nanoparticle surfaces interact with *S*-nitrosothiols (RSNO) through sulphur atom.

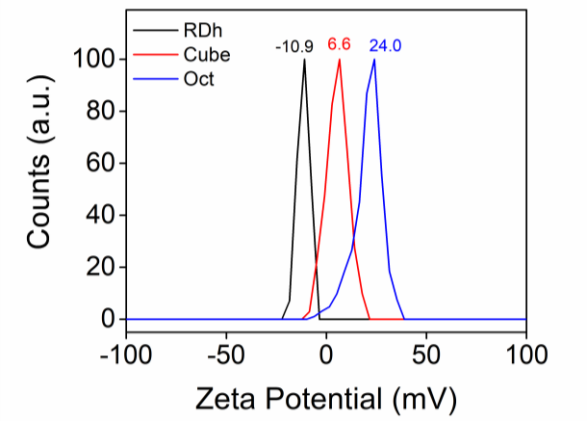

Fig. S21 Zeta (ζ) potential of Cu_2O nanomaterials. Measurements were done three times and the average values have been reported.

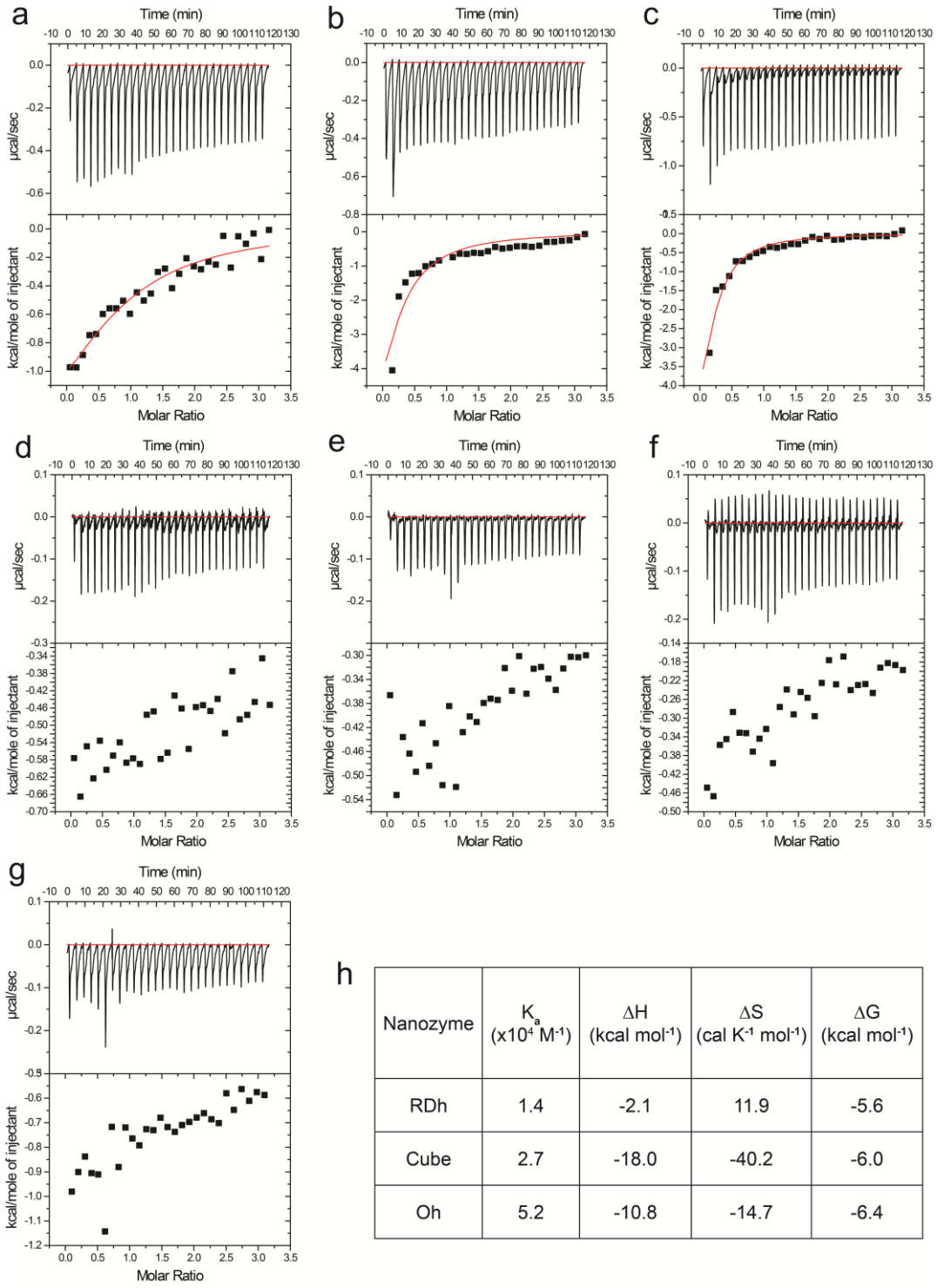

h

Nanozyme	K_a ($x10^4$ M^{-1})	ΔH (kcal mol^{-1})	ΔS (cal K^{-1} mol^{-1})	ΔG (kcal mol^{-1})
RDh	1.4	-2.1	11.9	-5.6
Cube	2.7	-18.0	-40.2	-6.0
Oh	5.2	-10.8	-14.7	-6.4

Fig. S22 Isothermal titration calorimetry (ITC) profile for binding GSH at 298 K by Cu_2O nanomaterials. a), b) and c) are the titration profile of catalyst (10 ng μl^{-1} or 0.07 mM, considering molar mass of Cu_2O is 143 g mol^{-1}) RDh, cube and Oh respectively with 1.0 mM GSH. d-f) Control titrations for RDh, cube and Oh respectively without GSH. g) Control titration with 1.0 mM GSH in the absence of any catalyst. The original titration profile (top) and the integrated heat (below) of each reaction are shown. h) Thermodynamic parameters obtained from ITC experiments were obtained using one-site binding model.

References

(1) (a) W. R. Mathews and S. W. Kerr, *J. Pharmacol. Exp. Ther.*, 1993, **267**, 1529-1537; (b) M. P. Gordge, J. S. Hothersall and A. A. Noronha-Dutra, *Br. J. Pharmacol.*, 1998, **124**, 141-148.

(2) A. Sahai, N. Goswami, S. D. Kaushik and S. Tripathi, *Appl Surf Sci*, 2016, **390**, 974-983.

(3) (a) S. Poulston, P. M. Parlett, P. Stone and M. Bowker, *Surf. Interface Anal.*, 1996, **24**, 811-820; (b) M. C. Biesinger, L. W. M. Laua, A. R. Gerson and R. C. Smart, *Appl Surf Sci*, 2010, **257**, 887-898.